The binding properties of the H5N1 influenza virus neuraminidase as inferred from molecular modeling

Michal Raab, Igor Tvaroška

The binding properties of the H5N1 influenza virus neuraminidase as inferred from molecular modeling

Received: 27.07.2010 / **Accepted:** 02.09.2010

Michal Raab and Igor Tvaroška✉

Institute of Chemistry, Centre for Glycomics, Slovak Academy of Sciences, Dúbravská cesta 9, 845 38 Bratislava, Slovak Republic

✉Tel.: +421 25941 0322; fax: +421 25941 0222; Email: chemitsa@savba.sk

Abstract

The avian influenza H5N1 virus has emerged as an important pathogen, causing severe disease in humans and posing a pandemic threat. Substrate specificity is crucial for the virus to obtain the ability to spread from avian to human. Therefore, an investigation of the binding properties of ligands at the molecular level is important for understanding the catalytic mechanism of the avian influenza virus neuraminidase and for designing novel and specific inhibitors of H5N1 neuraminidase. Based on the available crystal structure of H5N1, we have characterized the binding properties between sialic acid, methyl 3'sialyllactoside, methyl 6'sialyllactoside and the H5N1 influenza virus neuraminidase using molecular docking and molecular dynamics simulations. Obtained molecular dynamics trajectories were analyzed in terms of ligand conformations, N1-ligand interactions, and in terms of loop flexibility. It was found that in the N1-SA complex the sialic acid ring undergoes a transition from the $B_{2,5}$ to the $^{2}C_{5}$ conformation. However, in the N1-3SL and N1-6SL complexes sialic acid remained in the distorted boat conformation. The obtained results indicate that 3SL has only weak interactions with the 150-loop, whereas the N1-6SL complex shows strong interactions. Most of the differences arise from the various conformations around the glycosidic linkage, between the sialic acid and galactose, which facilitate the above interactions of 6SL with the enzyme, and as a consequence the interactions between the 150- and 430- loops. This finding suggests that the altered flexibility of loops in and around the active site is one of the reasons why the avian N1 preferentially cleaves sialic acid from α-(2-3)-Gal glycoconjugates over α-

(2-6)-Gal. These molecular modeling results are consistent with available experimental results on the specificity of N1.

Keywords H5N1 influenza virus · N1 neuraminidase · Molecular modeling · Binding properties · Sialic acid methyl 3'sialyllactoside · Methyl 6'sialyllactoside

Introduction

Influenza virus is a negative stranded RNA virus of the *Orthomyxoviridae* family, and based on serological differences, there are three distinct types of influenza viruses: A, B, and C. Influenza A viruses are the most widespread and infect many animal species. In humans, influenza viruses are common pathogens of the upper respiratory tract, and seasonal epidemics affect 10-20% of the general population. The emergence of new influenza strains in the human population occurs via transmission from other animal species, most notably birds. Transmission to humans is most commonly thought to occur through an intermediate host such as swine [1]. Typically, human and avian viruses are quite different and are not infectious for both species. Occasionally, direct avian-human transmission can occur with deadly results. Several instances of viral transmission from domestic chickens to humans have proven to be fatal, but no documented case of human to human transmission has occurred.

The influenza virus contains two surface antigenic glycoproteins, hemagglutinin (HA) and neuraminidase (NA, sialidase, *N*-acylneuraminate glycohydrolase, EC 3.2.1.18), and their functions in the infective cycle of influenza are well understood. These two glycoproteins are used to cluster influenza viruses into subtypes: 16 for HA (H1-H16) and 9 for NA (N1-N9). HA is responsible for binding to glycoconjugate moieties that contain terminal 5-*N*-neuraminic acid (sialic acid) on the surface of host cells. Influenza virus isolates from human strains bind preferentially to terminal sialic acids containing α-(2-6)-Gal structures, whereas avian and equine strains bind preferentially to α-(2-3)-Gal structures [2]. It is noteworthy that a single amino acid mutation is sufficient to change receptor specificity [3]. After replication of the virus, progeny virions bud from the cell surface and the role of a neuraminidase is to cleave terminal sialic acid moieties from the glycoconjugate receptors. This process facilitates elution of progeny virions from the infected cell and is critical for viral replication. Neuraminidases, of the type A viruses, are subdivided into two phylogenetically distinct families, group-1 and group-2. In contrast to hemagglutinin, there is only limited information on neuraminidase substrate specificity, though it has been suggested that neuraminidase preferentially recognizes the same linkage of sialic acid as the hemagglutinin of these viruses [4-6].

Structural analysis of influenza virus neuraminidase [7], and neuraminidase in complex with sialic acid [8], led to the design of a potent inhibitor of neuraminidase activity: zanamivir [9].

Based on the efficacy of zanamivir (Relenza^{TM}), another neuraminidase inhibitor was also developed: oseltamivir phosphate (Tamiflu^{TM}) [10]. Both Relenza^{TM}, a carbohydrate-based drug, and Tamiflu^{TM}, a carbocyclic mimetic, are potent and clinically effective anti-influenza drugs [11]. Despite the efficacy of these drugs, major concerns remain regarding the development of resistance to these drugs, which is already occurring [12, 13]. As a result of the emergence of the most recent avian influenza [14], caused by the H5N1 virus, it is commonly believed that influenza pandemics affecting humans are possible if the H5N1 virus acquires the ability to spread from human to human. Therefore, the development of a new arsenal of antiviral drugs is needed to deal with the H5N1 virus and its mutant forms [15, 16]. Recently, the crystal structure of H5N1 avian influenza neuraminidase (N1) was determined in apo form and in a complex with two drugs, oseltamivir and zanamivir [17]. A comparison of N1 (group-1) structures with the structures of other neuraminidases revealed that even though the binding location of oseltamivir is similar, there are relevant differences in the active site structure between group-1 (e. g. N1 and N4) and group-2 (e. g. N2 and N9) neuraminidases. This finding provides a new opportunity to design specific neuraminidase inhibitors. However, many questions still remain unanswered concerning the details of sialic acid binding and substrate specificity of the H5N1 influenza virus neuraminidase.

Given that the structure of sialic acid bound into N1 is not available, and N1 complexes with natural (reactive) substrates are less easily observed, computational modeling provides an alternative exploratory tool. In this study we attempt to answer the following question: is there any difference between the binding mode and behavior of three ligands (sialic acid and two trisaccharides, in which terminal sialic acid is α-ketosidically linked to lactose by α-(2-3)- and α-(2-6)-Gal linkage, respectively) into the active site of N1 neuraminidase? While there are several modeling studies on binding inhibitors to N1 neuraminidase [18-20], as far as we are aware, the above question was not investigated. To address this issue, we built and optimized three ligands using density functional theory (DFT) implemented in the Jaguar program [21]. Subsequently, the complexes of sialic acid and two trisaccharides bound into N1 neuraminidase were generated using a docking approach. Finally, we investigated the binding behavior of these ligands using molecular dynamics method. The results were analyzed in terms of N1-ligand interactions. Such information should be useful for the design of neuraminidase inhibitors, specific against group-1 and group-2 neuraminidases, respectively.

Computational methods

Ligands

The structures of the three investigated ligands (Fig. 1), namely sialic acid (5-*N*-acetyl-3,5,dideoxy-D-*glycero*-D-*galacto*-2-nonulosonic acid, neuraminic acid, α-Neu5Ac, SA), methyl 3'sialyllactoside (α-Neu5Ac-2,3-β-Gal-1,4-β-Glc-OMe, 3SL), and methyl 6'sialyllactoside (α-Neu5Ac-2,6-β-Gal-1,4-β-Glc-OMe, 6SL) were generated and subsequently fully optimized at the M05-2X [22] (DFT) level using the 6-31G* basis set [21]. Crystallographic studies of the neuraminidase-Neu5Ac complex showed [23] a distortion of the $^{2}C_{5}$ chair ring conformation into a boat conformer. Therefore, we have used the $^{2,5}B$ conformation as the starting conformation for the six-member SA ring. The ESP partial charges were computed at the same level of theory and were fitted to the atom centers. The Jaguar program [21], within the Schrödinger suite, was used for all computations. Dihedral angle are defined as follows, Φ_3= Φ(O6-C2-O2-C3'), Ψ_3 = Ψ(C2-O2-C3'-C4') for methyl 3'sialyllactoside; Φ_6=Φ(O6-C2-O2-C6'), Ψ_6=Ψ(C2-O2-C6'-C5'), and ω=ω(O2-C6'-C5'-O5') for methyl 6'sialyllactoside.

Docking

The Glide [24] module from the Schrödinger software package was used for docking the optimized ligands into N1 and the results were analyzed in the Pose Viewer utility within the package. The enzyme structure was based on the crystal structure of N1 in the closed form [17] (pdb code 2HU4). The X-ray crystallographic coordinates of N1 at a 2.5 Å resolution were acquired from the Protein Data Bank [25] and modified as follows. The previous study showed that monomer subunits within the tetramer behave independently [18], therefore the protein has been reduced to one monomer unit and the protein preparation was carried out using the Schrödinger [24] software package, which included water removal, hydrogen addition, protonation state correction and side chain optimization in the OPLS2001 force field [26, 27]. The Glide module utilizes an algorithm, which generates conformers of ligand molecules with up to 35 rotatable bonds. Thus during docking procedure orientations of all rotatable groups of ligands, between 11 and 24, are optimized to fit into the active site. The docking procedure consists of three steps. The initial step of Glide's docking algorithm involves filtering all the generated poses that do not meet the spatial requirements of the rigid

docking site of the receptor. The next step evaluates the ligand-receptor interaction energies using the GlideScore (G-Score) [28] empirical function. The last step is to evaluate and optimize the ligand-receptor non-bonding interaction energies in a grid approximation of the OPLS2001 force field. For the final scoring, the G-Score default function was used. The grid map was generated without scaling the charges and the Van der Waals radii. The ligands were placed in a 23x23x23 Å box around the position of the OTV molecule present in the crystal structure. The Van der Waals radius of the non-polar parts of the ligand with the atomic charges less than 0.15 was scaled by the factor of 0.8. 5000 generated conformations of each ligand were kept for the docking procedure, with the scoring window of 100 kcal mol^{-1}. The RMSD threshold for clustering of the docked poses was set to 0.5 Å and poses with the maximum atomic displacement less than 1.3 Å were discarded. The first 100 poses were energy minimized in the OPLS2001 force field. The 20 best poses of each run were visually inspected to determine the proper orientation of the ligand towards relevant amino acid residues.

Molecular dynamics simulations

Starting coordinates for molecular dynamics (MD) simulations were taken from the results of previous docking of SA, 3SL, and 6SL, respectively, into the crystal structure of N1. The initial coordinates and topology files were generated with the xLeap module within the AMBER 10 software suite [29]. Disulfidic bonds were explicitly defined for the relevant cysteines. The N1-ligand complexes were solvated with a TIP3P water model, creating a 15 Å solvation shell around the protein. Each system was then neutralized by the addition of sodium cations. The final systems contained approximately 40 000 atoms in a cubic box, with one side equaling 73 Å. The force field was based on ff99SB [30] along with the Glycam06 [31] carbohydrate parameters. In these simulations, an all-atom representation of hydroxyl was used to prevent undue distortion of the 3SL and 6SL trisaccharide structures in the vicinity of the charged enzyme residues. For all MD simulations, the AMBER 10 software package was used [29].

The relaxation procedure consisted of several steps. First, the hydrogen atoms and then the water molecules of the system were energy minimized, while keeping the rest of the system restrained. Afterwards, the system was energy minimized without constraints. To equilibrate the system, a series of four 100 ps constrained MD runs preceded the actual simulation,

lowering the constraints on the protein from 50 kcal mol^{-1} to 5 kcal mol^{-1} and, simultaneously, slowly heating the system up to 300K. The main MD run continued at 300K and constant pressure (NTP ensemble) for 25 ns. Langevin dynamics with the Leapfrog algorithm was employed to propagate the dynamics with a collision factor of 4 ps^{-1}. The integration time step was 1 fs and the data was collected every 1000 steps. The cut off for the nonbonding interactions was 10 Å and the long-range electrostatics were treated with the PME method. The analysis of the MD trajectory was carried out using tools within AMBER [29], and the VMD package [32] was used for visualization.

Results and discussion

Docking

The M05-2X/6-31G* optimization of three ligands (SA, 3SL, and 6SL), starting from the $^{2,5}B$ conformation in vacuum, led to minor conformational changes of the pyranose ring. In the SA, the initial $^{2,5}B$ conformation changed to $^{6}S_2$ (Cremer-Pople puckering parameters [33] φ=90.2°, θ=88.7°, and Q=0.78). In the 3SL, the ring conformation leaned towards $B_{2,5}/E_5$ (Cremer-Pople puckering coordinates φ=69.4°, θ=100.7°, and Q=0.67), and in the 6SL, the ring conformation changed to $^{4}S_2$ (Cremer-Pople puckering parameters φ=24.6°, θ=100.3°, and Q=0.69). In comparison, the conformation of the sialic acid pyranose ring in the active site of N9 neuraminidase (pdb code 2C4L [25]) resembles to $B_{2,5}/^{4}S_2$ (corresponding puckering parameters φ=46,6°, θ=98.3°, and Q=0.66). The various conformations of the ligands resulted in different partial charge distributions and, therefore, the ESP partial charges of the optimized structures were fitted to the atom centers and used in the following docking procedure.

The optimized structures, shown on Fig. 2, were used to generate the structures of three N1-complexes using the docking procedure. The docked poses for each ligand were sorted according to their predicted affinity by the empirical scoring function G-Score. To select the proper location and orientation of the substrate in the active site of N1 from docked poses, the position of the oseltamivir molecule (OTV) in the N1-OTV crystal structure [17] was used as a guide. The predicted binding affinity of the N1-3SL and the N1-6SL complex was very similar, with the corresponding values of -8.32 kcal mol^{-1} and -8.01 kcal mol^{-1} respectively.

These computational results are consistent with available experimental results [4-6], though the difference is below the accuracy of the scoring function. The superposition of the top-ranking poses within the OTV crystal structure is shown on Fig. 3. The sialic acid residue in the N1-SA and N1-6SL complexes overlaps nearly perfectly with OTV, while in the N1-3SL complex the sialic acid pyranose ring is comparatively distorted and shifted. The lactose aglycon, in both the N1-3SL and N1-6SL complexes, points away from the active site in the same direction, and the two lactose disaccharides overlap reasonably well. A closer comparison of the docked poses versus the OTV binding mode revealed subtle details of the substrate conformation and its interactions with surrounding residues. Fig. 4 displays distances between sialic acid and relevant residues of N1, as well as the glycosidic dihedral angles around the glycosidic linkage between sialic acid and aglycon in the N1-3SL and N1-6SL complexes. Their values are summarized for the generated structures of ligand-N1 complexes in Table 1 and Table 2.

Interactions of the carboxylate with the arginine triad (Arg 118, Arg 292, and Arg 371), documented by the r_2, r_3 and r_4 distances, are assumed to be responsible for the stabilization of the boat conformer. An inspection of docked poses revealed that these distances are conserved throughout all poses. In the best pose of the N1-SA complex, the r_2, r_3 and r_4 distances are 5.03 Å, 3.97 Å, and 4.53 Å, respectively. Similar distances are found in the N1-6SL complex, where their corresponding values are 4.99 Å, 3.96 Å, and 4.54 Å, respectively. In the N1-3SL complex, the r_2, r_3 and r_4 distances are 5.49 Å, 4.34 Å, and 4.22 Å, respectively. A shifted location of the sialic acid pyranose ring in the N1-3SL complex, compared to other two complexes, is responsible for up to a 0.5 Å change in these distances. Surprisingly, in the N1-SA and N1-6SL models, these distances are almost identical to the ones observed in the N1-OTV crystal structure.

The r_1 (r = C2…O_{Y406}) and r_6 (r = O2…C_{D151}) represent the distance between the anomeric carbon (C2) and glycosidic oxygen (O2) of the sialic acid residue, and the oxygen and carbon atoms of two assumed catalytic residues, namely Tyr 406 and Asp 151, respectively. It is clear that the r_1 distance depends on the pyranose ring conformation of the substrate in the active site and varies from 2.9 Å in N1-OTV to 3.7 Å in N1-3SL. On the other hand, the r_6 distance, that characterizes the possible proton transfer from Asp 151 to the glycosidic oxygen, ranges from 3.7 Å in N1-6SL to 4.4 Å in N1-3SL. The r_8 distance describes the hydrogen bond between Arg 152 and the acetamide oxygen. This interaction is conserved in all ligands and ranges from 2.7 Å in N1-OTV to 3.0 Å in N1-3SL. The Tyr 347 residue,

unique to H5N1, forms a hydrogen bond with the carboxylate, and the r_5 distance of about 3.7 Å is found to be very similar in all complexes. The r_7 distance represents the interaction between Glu 276 carboxylate oxygen and the C9 hydroxyl of the glycerol chain. In N1-SA, the distance of 4.6 Å reflects the improper orientation of the C9 hydroxyl when forming a hydrogen bond with Glu 276. In the case of N1-3SL, this distance is smaller (4.4 Å), and the C8 hydroxyl is properly orientated for a hydrogen bond interaction with Glu 276. This is documented by the 1.73 Å distance between HO-9 and O_{E276}. In N1-6SL, a strong hydrogen bond was found between the C9 hydroxyl and Glu 276, documented by the distance r_7 = 3.5 Å, which corresponds to the 1.91 Å distance between H-O8 and O_{E276}. The Cremer-Pople puckering coordinates [33] of the sialic acid pyranose ring are summarized in Table 2. In N1-SA and N1-3SL, the sialic acid ring conformation corresponds to ^3S_O while in N1-6SL it resembles a $B_{2,5}/^6S_2$ ring form. The Φ dihedral angles around the anomeric bond are in agreement with the exo-anomeric effect [34] in both the N1-3SL (Φ = 50°, Ψ = -95°) and N1-6SL (Φ = 77°, Ψ = 174°, ω =103°) complexes.

Molecular dynamics simulations

The structure of the best pose for each substrate was used to generate the starting geometry for a series of MD simulations. Altogether, the following four simulations of 25 ns length were carried out:

A – MD simulation of the free enzyme;

B – MD simulation of the N1-SA complex;

C – MD simulation of the N1-3SL complex;

D – MD simulation of the N16SL complex.

The plot of root-mean-square-deviations (RMSD) of the protein Cα backbone atoms with respect to the crystal structure are shown on Fig. 5a for all simulations. It can be seen that the enzyme structure is stable in all simulations, averaging RMSD values of 1.5 – 2 Å after the initial 5 ns, and no other major differences between **A - D** simulations were observed. On the other hand, the RMSD plot of the sialic acid residue (Fig. 5b) in the **B**, **C**, and **D** simulations exhibits significant differences and reflects how the lactose residue affects the binding behavior of the sialic acid residue. Fig. 5b demonstrates the exceptionally high RMSD value

in the **B** simulation, approaching about 9 Å for the second half of the trajectory. This is in contrast to the **C** and **D** simulations where the RMSD has significantly smaller values of about 2.5 Å. This suggests that the binding mode of the sialic acid residue in the N1-3SL and N1-6SL complexes is much more stable compared to the N1-SA complex. Visual inspection reveals that SA, in the MD simulation **B**, adopts various conformations and binding modes. Alternatively, sialic acid residue in simulations **C** and **D** remains in the active site with little change from the initial binding mode. The different binding behavior of ligands agree with the fact that while 3SL and 6SL are substrates for the enzymatic reaction, sialic acid is the product of this reaction and at the completion of the catalytic reaction it leaves the N1 active site.

The calculated B-factors, shown in Fig. 6 for all simulations, complement the RMSD values (Fig. 5) and illustrate how the substrate binding influences the positional fluctuations of the enzyme residues. An inspection of B factors revealed that several enzymatic regions exhibit a noticeable flexibility. In agreement with an earlier experiment [17] and previous MD simulations [18-20], our results show that the 150-loop is very flexible and can exist in several conformations. We observed similar flexibility not only in the free form of the enzyme (simulation **A**) but also in the case of the N1-SA and N1-3SL complexes (simulations **B** and **C**). In these complexes we also found that the 430-loop exhibits a substantial amount of flexibility. On the other hand, in the N1-6SL complex (simulation **D**) these segments of the enzyme are considerably less flexible. Since the flexibility of the 150-loop is assumed to be linked with the activity of N1, this difference may also reflect a preferred specificity of N1 for the α-(2-3)-Gal structural moiety over the α-(2-6)-Gal moiety. However, it is noteworthy that residues 110-112 and 247-250 exhibit increased mobility only in the N1-6SL complex.

In order to characterize the binding modes of these ligands, the sialic acid ring conformation, Φ and Ψ dihedral angles, and selected distances between the sialic acid residue and the enzyme residues in the active site (see Fig. 4) were monitored during the MD simulations. Fig. 7 shows time dependence of these distances over 25 ns MD trajectories for the **B**, **C**, and **D** simulations, respectively. Substrate distortion from the chair to boat conformation seems to be a general feature of the catalytic mechanism of glycoside hydrolases [35]. Similarly, it is assumed that the enzymatic mechanism of influenza virus neuraminidase proceeds via a boat conformation of the sialic acid residue. This is supported by X-ray crystallographic data on the N2-SA complex [8]. However, the crystal structure of the N1 complex, with SA or with

reactive ligands, is not available. The calculated free energy surface of SA [36] revealed that conformational equilibrium of SA is very sensitive to its environment. It was found that in vacuum three ring forms, namely $^{2}C_{5}$, $B_{3,6}/^{2}S_{6}$, and $^{O}S_{3}$, are almost equally populated with the $B_{3,6}/^{2}S_{6}$ stabilized by an intramolecular hydrogen bond between the amide N-H bond and the carboxylate group. However, in aqueous solution the $^{2}C_{5}$ conformation is predicted as the dominant conformer. To shed some light on ring distortion in the active site of N1, we have analyzed the conformational behavior of the sialic acid ring during MD simulations using Cremer-Pople puckering coordinates.

In simulation **B**, the sialic acid residue does not keep its initial binding mode or ring conformation. The pyranose ring adopts the $^{2}C_{5}$ conformation for most of the trajectory (Fig. 8). This finding is somewhat surprising as the crystal structure of the neuraminidase N2 complex with sialic acid showed a boat conformation [8], even though N2 and N1 neuraminidases are structurally distinct [17]. Key interactions for binding sialic acid in the active site of neuraminidases are with three arginine residues (Arg 118, Arg 292, and Arg 371) and a glutamate residue (Glu 276). A comparison of sialic acid bound to N2 with those docked into N1 revealed important differences in the active site, especially in the case of Glu 276. In the N2 complex the carboxylate oxygen atoms are directed toward the C8 and C9 hydroxyl groups and are at a distance showing a hydrogen bond, while in the N1 complex the Glu 276 residue has a different conformation with a substantially larger distance from the glycerol (C9 and C8) hydroxyl groups. The differing orientations of Glu 276 in the N2 and N1 complexes with sialic acid is also supported by the observation that upon OTV binding the carboxylate of Glu 276 adopts a different conformation in N1 compared to N2 [17]. An inspection of time dependence of the r_7 distance on Fig. 7 shows that the carboxylate and glycerol hydroxyl groups move away from each other during MD simulation.

Only the interaction with Arg 371 remains conserved for the time of simulation from all the SA substrate interactions, with the arginine triad represented by r_2, r_3, and r_4. Time dependence of the r_1 distance, given on Fig. 7, shows that the position of the anomeric carbon does not change with respect to Tyr 406. However, in the second half of the simulation, sialic acid changes its orientation upside-down, and as a result the C2 hydroxyl points towards Tyr 406. Alternatively, the interactions with Tyr 347, represented by r_5, remain conserved for the time of the simulation. None of the interactions described by distances r_6 and r_8 are conserved. Altogether, these numbers demonstrate that sialic acid was not able to keep its

initial binding mode in the active site of N1. As a consequence, sialic acid only kept its interactions to Tyr 347 and Arg 371.

The N1-3SL complex (**C**) is characterized by the salt bridge interactions to Arg 292 and Arg 371 of the arginine triad, represented by the r_3 and r_4 distances. Arg 118 shows varying interactions to the C4 hydroxyl and Glu 269, and does not form a salt bridge to SA. The r_1 plot shows that the SA stays close to Tyr 406 at distance of about 5 Å. This distance is influenced mainly by the SA ring conformation. Distribution of the sialic acid ring conformations, shown on Fig. 8, revealed that while the $^{2}C_5$ ring form is still dominant, the $^{3,6}B/^{6}S_2$ region is populated more than in the N1-SA complex. The hydrogen bond between Tyr 347 and the sialic acid carboxylate, represented by r_5, is conserved in the first 14 ns of the simulation. For the period between 14.5 ns and 19 ns, the r_5 distance oscillates around the value of 5 Å. At the same time, Tyr 347 interacts alternatively with the carboxylate and the C-2 hydroxyl of galactose. After 20 ns, the distance r_5 increases significantly, up to 10 Å, and Tyr 347 changes its orientation. Consequently, the Tyr 347 hydroxyl interacts by forming hydrogen bonds only with the surrounding water molecules. It appears that the interaction of highly mobile Asp 151 with the glycosidic oxygen O2 is not very stable. This is illustrated by the r_6 distance that fluctuates between 8 Å and 15 Å (Fig. 7). On the other hand, it was found that the distance between the acetamide oxygen of sialic acid and Arg 152, which is the neighboring residue to Asp 151, remains conserved for most of the trajectory, as demonstrated by the r_7 plot. The distance between Glu 276 and the C9 hydroxyl (r_8) fluctuates within the range of 3 Å – 6 Å. A visual inspection reveals interactions of Glu 276 with the glycerol chain hydroxyls. These interactions are eventually mediated by water molecules. Altogether, in the N1-3SL complex sialic acid kept most of the crucial interactions involving the active site residues. The significantly higher stability of the skew/boat conformation of the pyranose ring, in the N1-3SL complex vs. the preferred $^{2}C_5$ conformation in the N1-SA complex, suggests possible stabilization of the energetically less favored ring conformation by the accommodation of a lactose residue by the surrounding loops.

In the N1-6SL complex (**D)**, the sialic acid exhibits a similar binding profile to the arginine triad as in the N1-3SL complex (Fig. 7). The interactions with Arg 292 and Arg 371 are conserved; Arg 118 also interacts with other adjacent residues. The r_1 distance is kept at about 3.7 Å for the prevailing time of the simulation, which is less than in the N1-3SL complex. This is caused by the dominant $B_{2,5}/^{6}S_2$ conformation of the sialic acid ring, which is also illustrated in Fig. 8. The r_5 distance between Tyr 347 and the sialic acid carboxylate shows an

increase to more than 5 Å after 5 ns of the simulation, and thus losing the initial hydrogen bond. A visual analysis shows varying interactions of Tyr 347 to the glycosidic oxygen and the C8 hydroxyl of the sialic acid during the period of 5 ns – 12 ns. After that, the Tyr 347 does not form a hydrogen bond to methyl 6'sialyllactoside and adopts a sandwich-like orientation in respect to the galactose ring. Similarly, as in both previously discussed N1-SA and N1-3SL complexes, the Asp 151 stays in the proximity of the glycosidic oxygen, as shown by the plot of r_6. In the N1-6SL complex, Asp 151 forms a strong hydrogen bond with Arg 430. The r_7 distance is conserved throughout the simulations, reflecting the hydrogen bond of Glu 276 with the C9 hydroxyl. An inspection of structures during the simulation revealed the formation of a strong hydrogen bond between Arg 152 and the C2 hydroxyl of the glucose residue (documented by the interatomic distance $r(NH_2...OH)$ of less than 2.5Å for 60% of the trajectory). This bond lasts for the rest of the simulation time, and we assume that this hydrogen bond facilitates stabilization of the C9···Glu 276 interactions. The r_8 distance exhibits a similar behavior to the N1-3SL complex and oscillates around 5 Å in the second half of the trajectory.

In MD studies on N1 in complex with several NA inhibitors [19, 20] it was found that Tyr 347 forms a hydrogen bond with a negatively charged group of inhibitors. It appears that in the case of the studied ligands, Tyr 347 also interacts with the hydroxyl groups of galactose. In contrast, the conformational behavior of the glycosidic linkage between SA and galactose influences the ability of Tyr 347 to interact with the sialic acid carboxylate, possibly due to the steric interactions imposed by the Glc and Gal residues. Consequently, interactions between Tyr 347 and galactose play an important role in the orientation of aglycon and vice versa. Analysis of glycosidic torsional angles showed that conformational behavior of the β-1-4-linkage between Gal and Glc is very similar in both trisaccharides. In fact, this linkage adopts a "standard" conformation with Φ_4(O5'-C1'-O4''C4'') and Ψ_4(C1'-O4''-C4''-C5'') angles of approximately -75° and -125°, respectively, and stays in the same energy minimum during the simulation. Essentially the same conformation has been recently identified as a local minimum of cellulose in solution [37]. Therefore, the key factor in determining an overall 3D structure (shape) of the 3SL and 6SL molecules is the conformation of the glycosidic linkage between the sialic acid and galactopyranose.

A scatterplot of the corresponding glycosidic torsional angles is shown on Fig. 9. As expected, it can be clearly seen that the α-2,6 linkage is more flexible than the α-2,3 linkage.

During the dynamics simulation, the α-2,6 linkage stayed in three low energy regions, characterized by the ±*gauche* and *trans* orientations of the Φ_6 angle and by the *trans* orientation of the Ψ_6 angle. The ω_6 dihedral angle remained in the region of 60° during the simulation. Conversely, the α-2,3 linkage stays in two regions characterized by the ±*gauche* orientation of the Φ_3 angle and by the *gauche* orientation of the Ψ_3 angle. It is noteworthy that the calculated conformations for the α-2,6 and α-2,3 linkages in complex with N1 are similar to conformers determined from NMR data [38, 39] for these structural moieties. Through NMR studies it was found [38] that the disaccharide α-Neu5Ac-2,3-β-Gal exists in solution as a mixture of two conformers with glycosidic dihedral angles (ϕ = -153º, ψ = -26 º) and (-85 º,120 º), where $\phi = \phi$(C1-C2-O2-C3'), and $\psi = \psi$(C2-O2-C3'-H3') respectively. For the 6SL trisaccharide it was found [39] that the α-2,6 linkage exists as an equilibrium of two conformers, with the *gauche* orientation of the Φ angle as the preferred one.

To clarify effects of substrate binding on the dynamic behavior of the surrounding loops, we performed a hydrogen bond analysis between the 150-, 247-, and 430-loops of N1 and the ligand's aglycon (Table 3). The comparison of hydrogen bonds between the Glc and Gal residues in the **C** and **D** simulations, respectively, points to different binding modes of the aglycon in the active site. In the N1-3SL complex (**C**), the aglycon prefers to bind to the 247-loop, which is demonstrated by a significant occurrence of hydrogen bonds between the lactose residue and Ser 246 and Asn 247. In the N1-3SL complex, the most significant interactions of the lactose aglycon with the surrounding residues seem to be the hydrogen bonds between Asn 247 and the C6 hydroxyl of galactose, and occasionally with the C3 hydroxyl of glucose. The relative occurrence of these hydrogen bonds is 34.6 % and 13.0 %, respectively. The C4 galactose hydroxyl was found to be involved in interactions with Tyr 347 (23.6 %). Interestingly, an intramolecular hydrogen bond between the galactose C4 hydroxyl and the SA C9 hydroxyl (33.4 %) was also observed. Formation of hydrogen bonds of glucose to Asp 151 and Arg 152 of the 150-loop is occasional, with relative occurrences of 6.4 %, and 4.6 %, respectively.

Unlike the N1-3SL complex, binding to the 150-loop is more frequent in the N1-6SL complex (**D**). This is demonstrated by hydrogen bond interactions of Glc to Arg 152 (17.4 %) and Asp 151 (29.6 %), respectively. Moreover, an inspection of hydrogen bond patterns during the MD simulations of the N1-6SL complex revealed the presence of hydrogen bond interactions between Arg 430 of the 430-loop and Asp 151 of the 150-loop (Fig. 10), with a calculated

occurrence of 49.2 %. These interactions are responsible for the exceptionally low mobility of both the 150-loop and the 430-loop in simulation **D**, as illustrated by the B-factors on Fig. 6. Moreover, this hydrogen bond decreases a nucleophilicity of the Asp 151 oxygen and thereby decreases its catalytic activity. Consequently, due to the mutual orientation of SA and glucose, intramolecular hydrogen bonds are formed between the C4 hydroxyl of sialic acid and the C3 hydroxyl of glucose (25.6 %), as well as between the *N*-acetyl group oxygen of sialic acid and the C2 hydroxyl of glucose (12.2 %).

In the absence of experimental studies on the detailed mechanism of the N1 specificity, the theoretical modeling can provide valuable information. Overall, our results indicate that the binding modes of 3SL and 6SL in the active site of N1 are clearly different. The calculations identified dominant specific interactions between Asn 247 and Tyr 347 with the substrate in the N1-3SL complex (**C**). On the contrary, the N1-6SL complex is characterized by the formation of hydrogen bonds of the aglycon residues Glc and Gal to the 150-loop, thereby weakening the interactions of Asp 151 to sialic acid. Furthermore, the results revealed interactions between the 150-loop and 430-loop that are responsible for decreased flexibility of the 150-loop in the N1-6SL complex. The dramatic difference in the preference of the glycosidic linkage conformation between the N1-3SL and N1-6SL complexes has a significant impact on the dynamics of the loops around the active site. As these loops carry some amino acid residues crucial for enzymatic function, one may speculate that this may be one of the reasons for the specificity of N1 for the substrate's linkage type. All of these results imply that the N1 enzyme of the avian influenza virus binds in the binding mode that facilitates preferential cleavage of sialic acid from methyl 3'sialyllactoside over methyl 6'sialyllactoside. These results are consistent with experimental data that showed that avian influenza virus desialylates α-Neu5Ac-2,3-linked oligosaccharides at least one order faster than α-Neu5Ac-2,6-linked oligosaccharides [6] and with the data on specificity of the human influenza virus neuraminidases [4, 5].

Summary

The present results elucidate the binding mechanics of sialic acid, methyl 3'sialyllactoside, and methyl 6'sialyllactoside into the H5N1 influenza virus neuraminidase using DFT quantum mechanics calculations, molecular docking techniques, and molecular dynamics simulations. Obtained molecular dynamics trajectories were analyzed in terms of ligand

conformations, hydrogen bond interactions between ligands and amino acid residues in the active site, and in terms of loop flexibility. The results of four, 25 ns molecular dynamics simulations showed that in the N1-SA complex the sialic acid ring undergoes a transition from the $B_{2,5}$ to the $^{2}C_{5}$ conformation, whereas in the N1-3SL and N1-6SL complexes sialic acid stayed in a distorted boat conformation. The obtained results indicate that 6SL has strong interactions with the 150-loop, whereas the N1-3SL complex shows only weak interactions. Most of the difference arises from distinct conformations around the glycosidic linkage between the sialic acid and galactose, which facilitates the above interactions in N1-6SL and as a consequence also the interactions between the 150- and 430- loop. These interactions are responsible for the different binding mode of 3SL and 6SL, respectively and as a consequence for the specificity of the H5N1 avian influenza virus neuraminidase, which preferentially destroys the α-Neu5Ac-2,3-β-Gal structural moiety. These molecular modeling results are consistent with available experimental results on the specificity of N1. The characterization of binding properties of the H5N1 active site could be used as a starting point for understanding the catalytic mechanism of avian influenza virus neuraminidases and in designing novel and specific inhibitors of H5N1 neuraminidase as potential therapeutics for the treatment of avian flu.

Acknowledgments

This investigation was supported by grants from the Slovak Research and Development Agency under contract APVV-0607-07, from VEGA (grant No. 2/0128/08) and from the Centers of Excellence program of the Slovak Academy of Sciences (COMCHEM, Contract no. II/1/2007).

References

1. Webster RG, Bean WJ, Gorman OT, Chambers TM, Kawaoka Y (1992) Evolution and Ecology of Influenza A Viruses. Microbiol Rev 56:152-179
2. Corfield AP, Higa H, Paulson JC, Schauer R (1983) The specificity of viral and bacterial sialidases for alpha(2-3)- and alpha(2-6)-linked sialic acids in glycoproteins. Biochim Biophys Acta 744:121-126
3. Rogers GN, Paulson JC (1983) Receptor determinants of human and animal influenza virus isolates: differences in receptor specificity of the H3 hemagglutinin based on species of origin. Virology 127:361-373
4. Franca de Barros J Jr, Sales Alviano D, da Silva MH, Dutra Wigg M, Sales Alviano C, Schauer R, dos Santos Silva Couceiro JN (2003) Characterization of sialidase from an influenza A (H3N2) virus strain: kinetic parameters and substrate specificity. Intervirology 46:199-206
5. Kobasa D, Kodihalli S, Luo M, Castrucci MR, Donatelli I, Suzuki Y, Suzuki T, Kawaoka Y (1999) Amino acid residues contributing to the substrate specificity of the influenza A virus neuraminidase. J Virol 73:6743-6751
6. Mochalova LV, Korchagina EY, Kurova VS, Shtyria JA, Gambaryan AS, Bovin NV (2005) Fluorescent assay for studying the substrate specificity of neuraminidase Anal Biochem 341:190-193
7. Varghese JN, Laver WG, Colman PM (1983) Structure of the influenza virus glycoprotein antigen neuraminidase at 2.9 Å resolution. Nature 303:35-40
8. Varghese JN, McKimm-Breschkin JL, Caldwell JB, Kortt AA, Colman PM (1992) The Structure of the Complex between Influenza-Virus Neuraminidase and Sialic-Acid, the Viral Receptor. Proteins: Struct Funct Genet 14:327-332
9. von Itzstein M, Wu WY, Kok GB, Pegg MS, Dyason JC, Jin B, Phan TV, Smythe ML, White HF, Oliver SW, Colman PM, Varghese JN, Ryan DM, Woods JM, Bethell RC, Hotham VJ, Cameron JM, Penn CR(1993) Rational Design of Potent Sialidase-Based Inhibitors of Influenza-Virus Replication. Nature363:418-423
10. Kim CU, Lew W, Williams MA, Liu HT, Zhang LJ, Swaminathan S, Bischofberger N, Chen MS, Mendel DB, Tai CY, Laver WG, Stevens RC(1997) Influenza Neuraminidase Inhibitors Possessing a Novel Hydrophobic Interaction in the Enzyme Active Site: Design, Synthesis, and Structural Analysis of Carbocyclic Sialic Acid Analogues with Potent Anti-Influenza Activity. J Am Chem Soc 119:681-690

11. McCullers JA, Hoffmann E, Huber VC, Nickerson AD(2005) A single amino acid change in the C-terminal domain of the matrix protein M1 of influenza B virus confers mouse adaptation and virulence. Virology 336:318-326
12. de Jong MD, Thanh TT, Khanh TH, Hien VM, Smith GJD, Chau NV, Cam BV, Qui PT, Ha DQ, Guan Y, Peiris JSM, Hien TT, Farrar J (2005) Oseltamivir Resistance during Treatment of Influenza A (H5N1) Infection. N Engl J Med 353:2667-2672
13. Kiso M, Mitamura K, Sakai-Tagawa Y, Shiraishi K, Kawakami C, Kimura K, Hayden FG, Sugaya N, Kawaoka Y (2004) Resistant influenza A viruses in children treated with oseltarnivir: descriptive study. Lancet 364:759-765
14. Li KS, Guan Y, Wang J, Smith GJD, Xu KM, Duan L, Rahardjo AP, Puthavathana P, Buranathai C, Nguyen TD, Estoepangestie ATS, Chaisingh A, Auewarakul P, Long HT, Hanh NTH, Webby RJ, Poon LLM, Chen H, Shortridge KF, Yuen KY, Webster RG, Peiris JSM (2004) Genesis of a highly pathogenic and potentially pandemic H5N1 influenza virus in eastern Asia. Nature 430:209-213
15. von Itzstein M (2007) The war against influenza: discovery and development of sialidase inhibitors. Nat Rev Drug Discovery 6:967-974
16. von Itzstein M (2008) Avian influenza virus, a very sticky situation. Curr Opin Chem Biol12:102-108
17. Russell RJ, Haire LF, Stevens DJ, Collins PJ, Lin YP, Blackburn GM, Hay AJ, Gamblin SJ, Skehel JJ (2006) The structure of H5N1 avian influenza neuraminidase suggests new opportunities for drug design. Nature 443:45-49
18. Amaro RE, Minh DDL, Cheng LS, Lindstrom WM, Olson AJ, Lin J-H, Li WW, McCammon JA (2007) Remarkable Loop Flexibility in Avian Influenza N1 and Its Implications for Antiviral Drug Design. J Am Chem Soc 129:7764-7765
19. Landon MR, Amaro RE, Baron R, Ngan CH, Ozonoff D, McCammon JA, Vajda S (2008) Novel Druggable Hot Spots in Avian Influenza Neuraminidase H5N1 Revealed by Computational Solvent Mapping of a Reduced and Representative Receptor Ensemble. Chem Biol Drug Des 71:106-116
20. Udommaneethanakit T, Rungrotmongkol T, Bren U, Frecer V, Stanislav M (2009) Dynamic Behavior of Avian Influenza A Virus Neuraminidase Subtype H5N1 in Complex with Oseltamivir, Zanamivir, Peramivir, and Their Phosphonate Analogues. J Chem Inf Model 49:2323-2332
21. Schrödinger, LLC (2008) Jaguar, version 7.5, New York, NY

22. Zhao Y, Schultz NE, Truhlar DG (2006) Design of Density Functionals by Combining the Method of Constraint Satisfaction with Parametrization for Thermochemistry, thermochemical Kinetics, and Noncovalent Interactions. J Chem Theory Comput 2:364-382
23. Varghese JN, Smith PW, Sollis SL, Blick TJ, Sahasrabudhe A, McKimm-Breschkin JL, Colman PM (1998) Drug design against a shifting target: a structural basis for resistance to inhibitors in a variant of influenza virus neuraminidase. Structure 6:735-746.
24. Schrödinger, LLC (2007) Glide, version 4.5. New York, NY
25. Bernstein FC, Koetzle TF, Williams GJB, Meyer EF, Brice MD, Rodgers JR, Kennard O, Shimanouchi T, Tasumi M (1977) The Protein Data Bank: a computer-based archival file for macromolecular structures. Arch Biochem Biophys112:535-542
26. Jorgensen WL, Maxwell DS, Tirado-Rives J,(1996) Development and Testing of the OPLS All-Atom Force Field on Conformational Energetics and Properties of Organic Liquids. J Am Chem Soc 118:11225-11236
27. Kaminski GA, Friesner RA, Tirado-Rives J, Jorgensen WL (2001) Evaluation and Reparametrization of the OPLS-AA Force Field for Proteins via Comparison with Accurate Quantum Chemical Calculations on Peptides. J Phys Chem B 105:6474-6487
28. Friesner RA, Murphy RB, Repasky MP, Frye LL, Greenwood JR, Halgren TA, Sanschagrin PC, Mainz DT (2006) Extra Precision Glide: Docking and Scoring Incorporating a Model of Hydrophobic Enclosure for Protein−Ligand Complexes. Journal of Medicinal Chemistry 49:6177-6196
29. Case DA, Darden TA, Cheatham III TEC, Simmerling CL, Wang J, Duke RE, Luo R, Crowley M, Walker RC, Zhang W, Merz KM, Wang B, Hayik S, Roitberg A, Seabra G, Kolossváry I, Wong KF, Paesani F, Vanicek J, Wu X, Brozell SR, Steinbrecher T, Gohlke H, Yang L, Tan C, Mongan J, Hornak V, Cui G, Mathews DH, Seetin MG, Sagui C, Babin V, Kollman PA (2008) AMBER 10. University of California: San Francisco.
30. Hornak V, Abel R, Okur A, Strockbine B, Roitberg A, Simmerling C (2006) Comparison of multiple Amber force fields and development of improved protein backbone parameters. Proteins 65:712-725
31. Kirschner KN, Yongye AB, Tschampel SM, Gonzalez-Outeirino J, Daniels CR, Foley BL, Woods RJ (2008) GLYCAM06: a generalizable biomolecular force field. Carbohydrates. J Comput Chem 29:622-655
32. Humphrey W, Dalke A, Schulten K (1996) VMD: visual molecular dynamics. J Mol Graphics Modell 14:33-38, 27-38

33. Cremer D, Pople JA (1975) General definition of ring puckering coordinates. J Am Chem Soc. 97:1354-1358
34. Tvaroška I, Carver JP (1997) Ab Initio Molecular Orbital Calculation of Carbohydrate Model Compounds. 6. The Gauche Effect and Conformations of the Hydroxymethyl and Methoxymethyl Groups. J Phys Chem B 101:2992-2999
35. Vocadlo DJ, Davies GJ (2008) Mechanistic insights into glycosidase chemistry. Curr Opin Chem Biol 12:539-555
36. Spiwok V, Tvaroska I (2009) Conformational Free Energy Surface of alpha-N-Acetylneuraminic Acid: An Interplay Between Hydrogen Bonding and Solvation. J Phys Chem B 113:9589-9594
37. Shen T, Langan P, French AD, Johnson GP, Gnanakaran S (2009) Conformational Flexibility of Soluble Cellulose Oligomers: Chain Length and Temperature Dependence. J Am Chem Soc 131:14786-14794
38. Poppe L, Dabrowski J, Lieth C-W, Numata M, Ogawa T(1989) Solution conformation of sialosylcerebroside (G_{M4}) and its NeuAc(α2→3)Galβ sugar component. Eur J Biochem 180:337-342
39. Poppe L, Stuike-Prill R, Meyer B, van Halbeek H (1992) The solution conformation of sialyl-alpha (2----6)-lactose studied by modern NMR techniques and Monte Carlo simulations. J Biomol NMR 2:109-136

Tables

Table 1 Calculated distances (in Å) of the selected interactions of the docked poses of Neu5Ac (SA), Neu5Ac-3-Gal-4-Glu-OMe (3SL), and Neu5Ac-6-Gal-4-Glu-OMe (6SL) in N1. The oseltamivir (OTV) crystal structure is used as a reference

	r_1	r_2	r_3	r_4	r_5	r_6	r_7	r_8
N1-OTV	2.87	5.21	3.95	4.55	3.66	-	-	2.65
N1-SA	3.29	5.03	3.97	4.53	3.72	3.81	4.62	2.85
N1-3SL	3.73	5.49	4.34	4.22	3.78	4.39	4.42	3.03
N1-6SL	3.45	4.99	3.96	4.54	3.76	3.72	3.51	2.81

Table 2 Measured Cremer-Pople angular puckering coordinates **Θ** and **φ** of the sialic acid pyranose ring in the docked poses of Neu5Ac (SA), Neu5Ac-3-Gal-4-Glu-OMe (3SL), and Neu5Ac-6-Gal-4-Glu-OMe (6SL) and the glycosidic dihedral angles **Φ**,**Ψ**, and **ω** in Neu5Ac-3-Gal (3SL) and Neu5Ac-6-Gal (6SL). All angles are in degrees

	Θ	**φ**	**Φ**	**Ψ**	**ω**
SA	76.1	302.4	-	-	-
3SL	92.3	296.8	49.7	-95.1	-
6SL	93.2	15.4	77.2	-173.5	102.9

Table 3 Hydrogen bonds[a] between the substrate's aglycon residues and residues of the 150-loop and the 247-loop in models N1-3SL and N16-SL

	Asp151		Arg 152		Asn 247		Tyr 347		Neu5Ac	
	C	**D**	**C**	**D**	**C**	**D**	**C**	**D**	**C**	**D**
Gal	0	0.6	0	0	34.6	0	23.6	2.6	33.4	0.6
Glc	6.4	29.6	4.6	17.4	13	0	0	0	0	37.8

[a] Hydrogen bond occurences are given in percentage (%) and is defined as the number of H-bonds per MD frame. The data for the analysis was collected in 500 ps intervals and the hydrogen bond was defined by a 3.5 Å distance and 20° angle treshold between the hydrogen donor and acceptor

Figure captions

Fig. 1 The chemical structures of the studied ligands: sialic acid (5-*N*-acetyl-3,5,dideoxy-D-*glycero*-D-*galacto*-2-nonulosonic acid, neuraminic acid, α-Neu5Ac, SA), methyl 3'sialyllactoside (α-Neu5Ac-2,3-β-Gal-1,4-β–Glcu-OMe, 3SL), and methyl 6'sialyllactoside (α-Neu5Ac-2,6-β-Gal-1,4-β–Glc-OMe, 6SL)

Fig. 2 The M05-2X/6-31G* optimized structures of the ligands used for a generation of the enzyme-ligand complexes: sialic acid (SA), methyl 3'sialyllactoside (3SL), and methyl 6'sialyllactoside (6SL)

Fig. 3 Superposition of the docked ligands and OTV in the active site of the N1 crystal structure. The enzyme is shown as a grey surface representation and ligands are shown in stick representation with the Connolly surface; OTV is colored grey, SA is green, 3SL is red, and 6SL is black

Fig. 4 Schematic representation of interactions of ligands within the active site of N1. The distances are selected to monitor the interactions between the ligand and N1, and the dihedral angles Φ/Ψ and Φ/Ψ/ω describing the glycosidic linkage are defined as C3'-O3'-C2-O6/C2'-C3'-O3'-C2, and C6'-O6'-C2-O6/C5'-C6'-O6'-C2/O5'-C5'-C6'-O6', respectively

Fig. 5 Mass-weighted RMSD time dependence of the Cα atoms (a) and atoms of the sialic acid residue (b) during the **A**, **B**, **C**, and **D** simulations

Fig. 6 Calculated B-factors for the enzyme residues in the **A**, **B**, **C**, and **D** simulations

Fig. 7 Time dependence of r_1 - r_8 distances representing selected interactions between the enzyme residues and ligand atoms in the **B**, **C**, and **D** simulations. Distances are described in Fig. 4

Fig. 8 Scatterplots of the ring conformation for the six-member ring of sialic acid represented by the Cremer-Pople puckering coordinates (top) and its z-axis

projection in two-dimensions (bottom) during the **B**, **C**, and **D** simulation, respectively. Conformational space sampling started from the $^{2,5}B$ conformation

Fig. 9 Scatterplot of the glycosidic dihedral angles between sialic acid and galactose, calculated from the 25 ns MD simulations of N1-3SL(simulation C) and N1-6SL (simulation D) complexes, respectively

Fig. 10 Snapshot of the N1-6SL complex from the MD simulation at 15 ns. Ribbon representations of the 150-loop and the 430-loop (red) are superposed with the corresponding loops in the N1 crystal structure (green). Amino acid residues D151 and R430, and the bound substrate 6SL, are shown in stick representation. Dashed lines represent the hydrogen bond between R430 and D151

Figure 1

Click here to download high resolution image

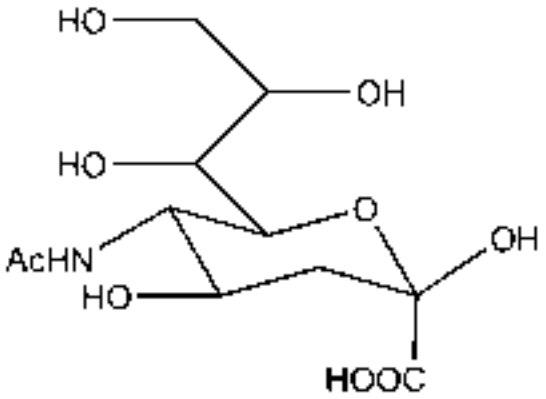

sialic acid

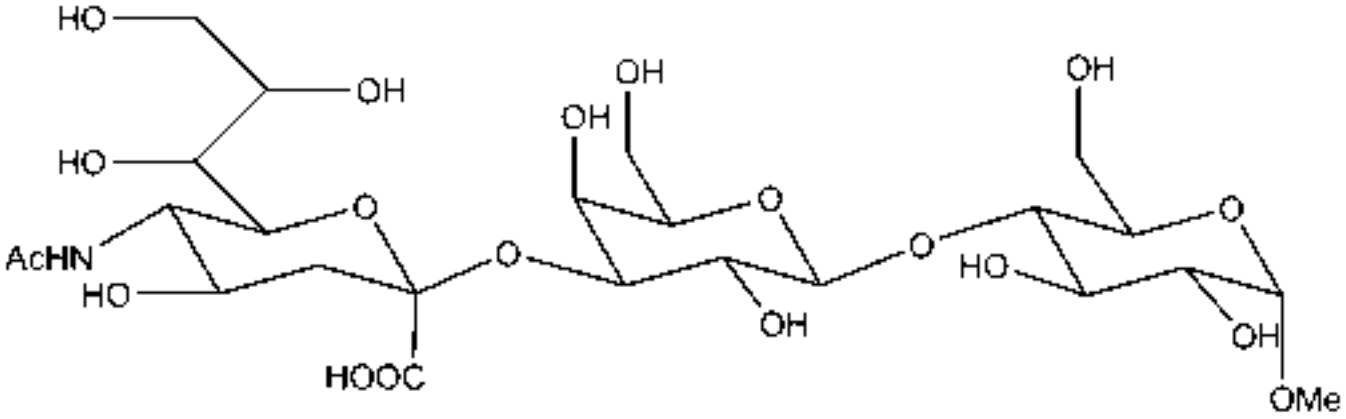

methyl 3'sialyllactose

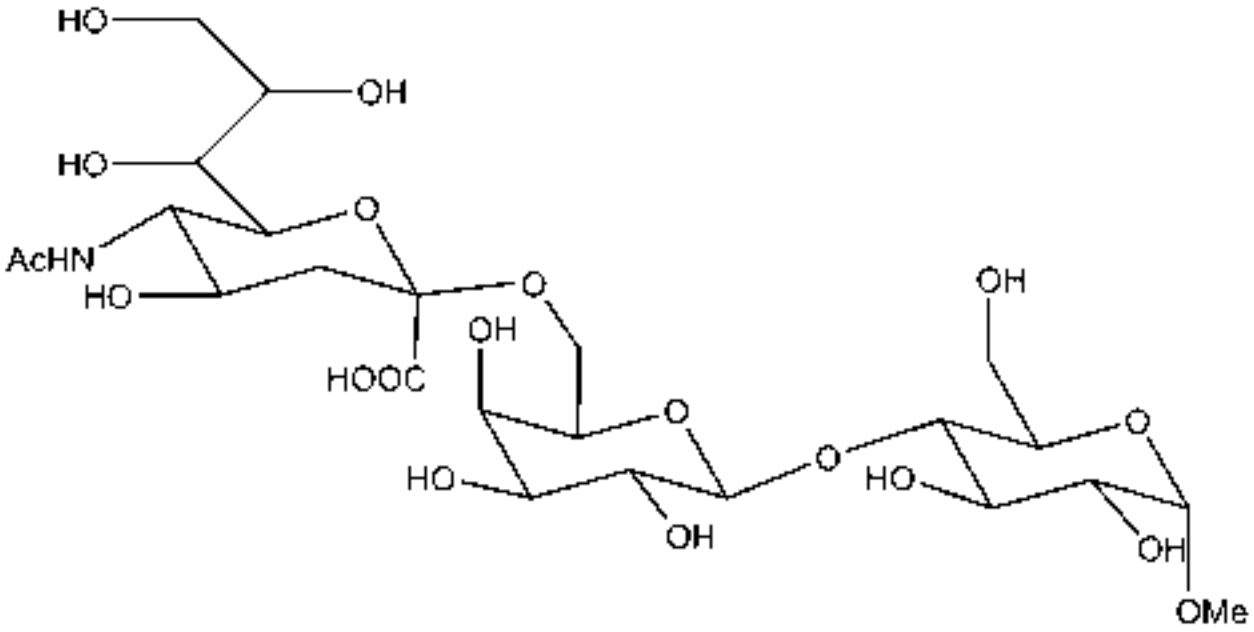

methyl 6'sialyllactose

Figure 2

Click here to download high resolution image

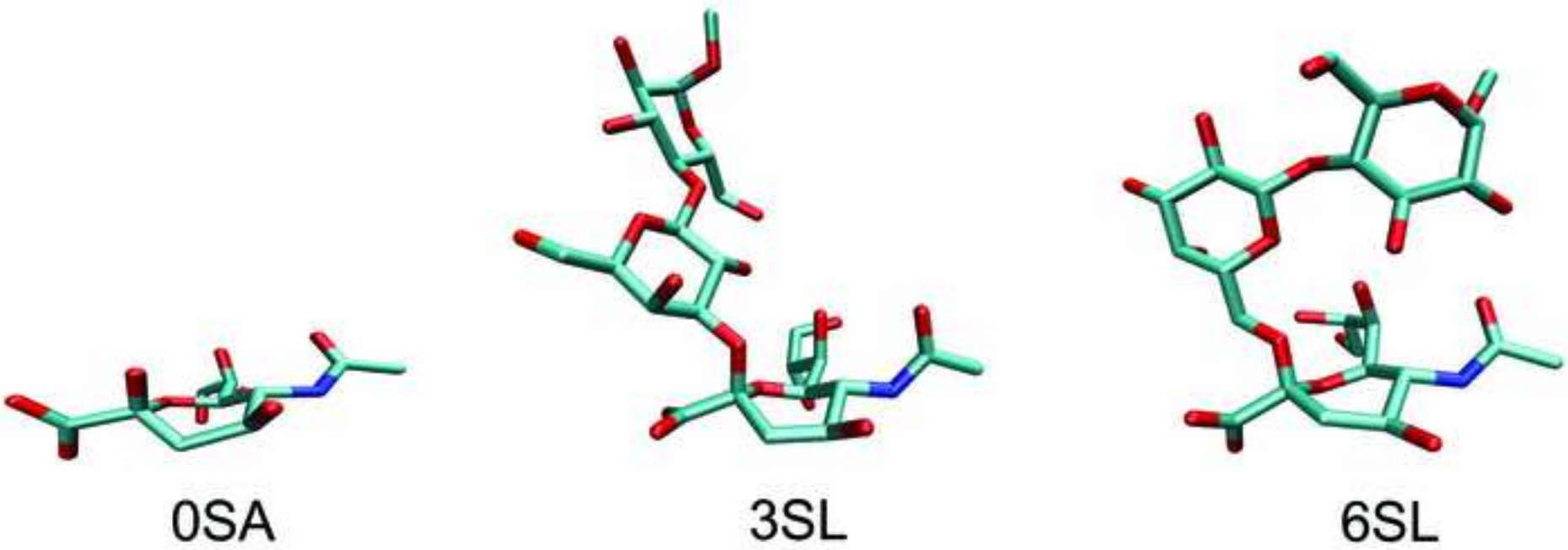

Figure 3
Click here to download high resolution image

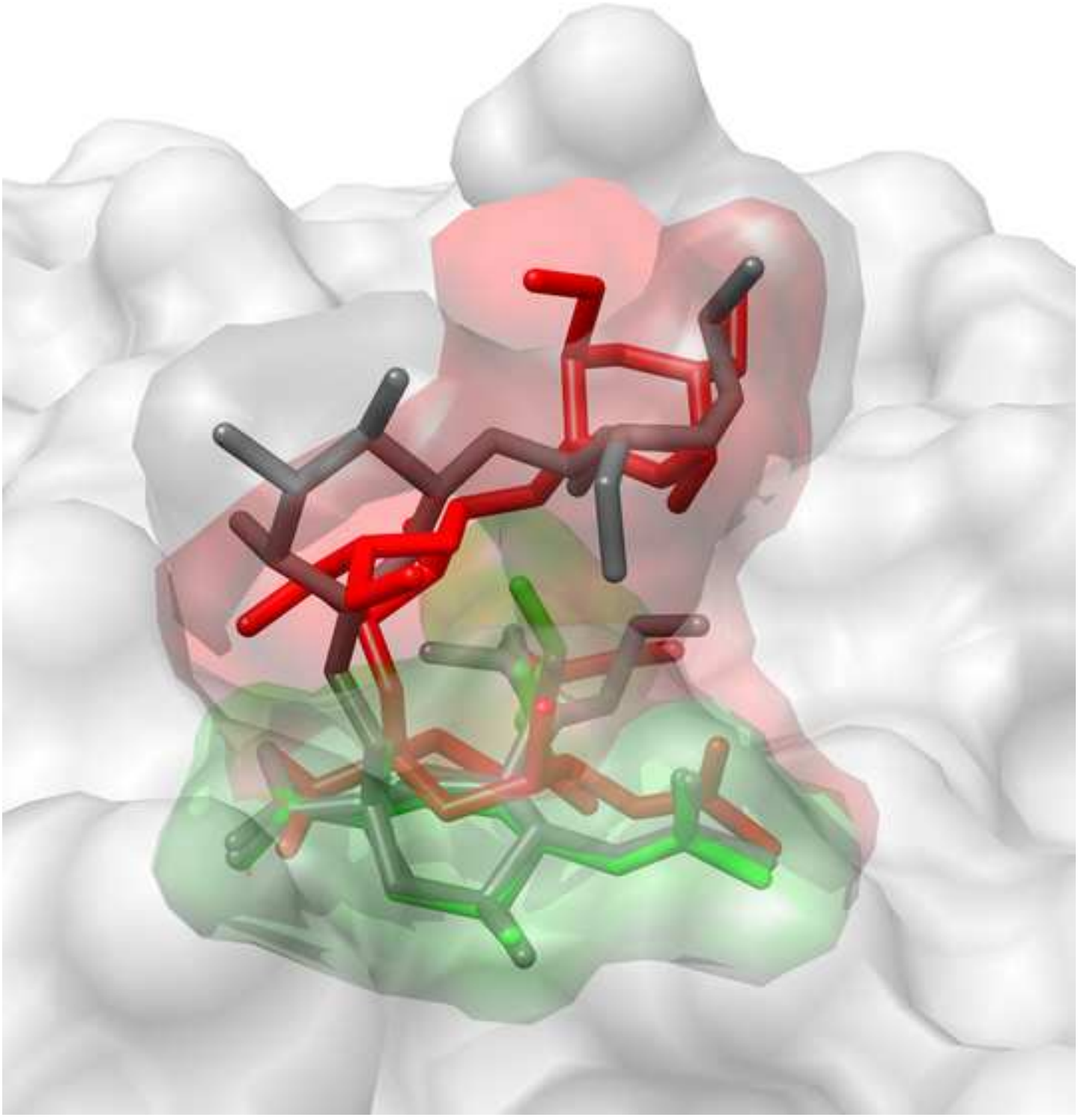

Figure 4

Click here to download high resolution image

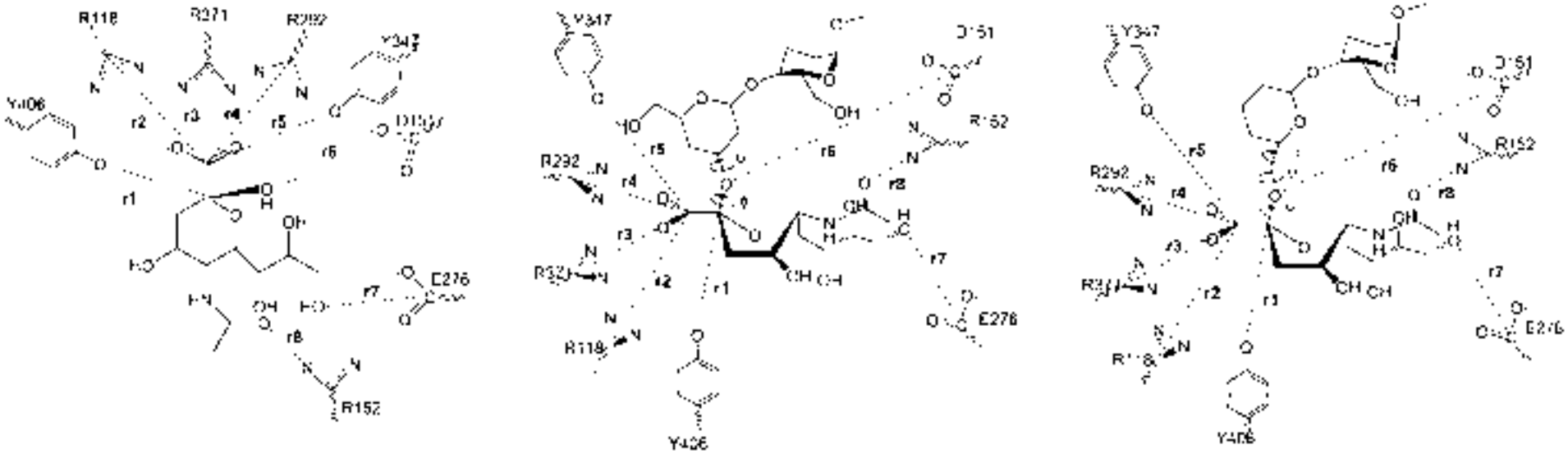

Figure 5
Click here to download high resolution image

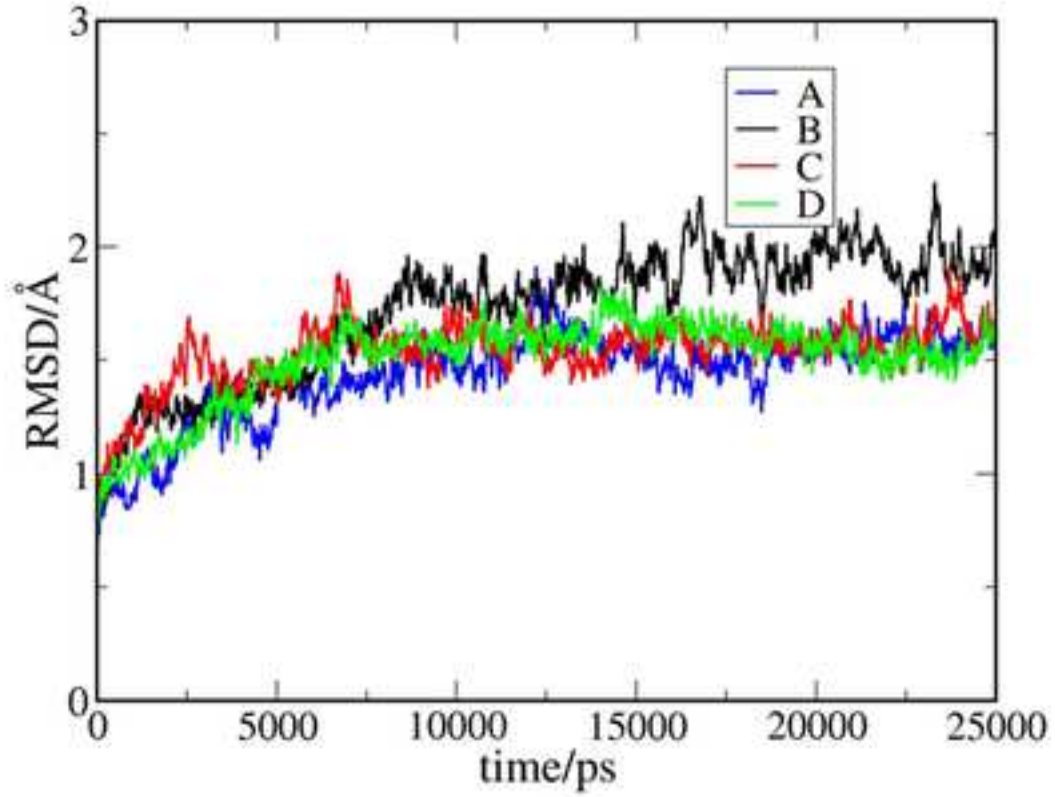

a)

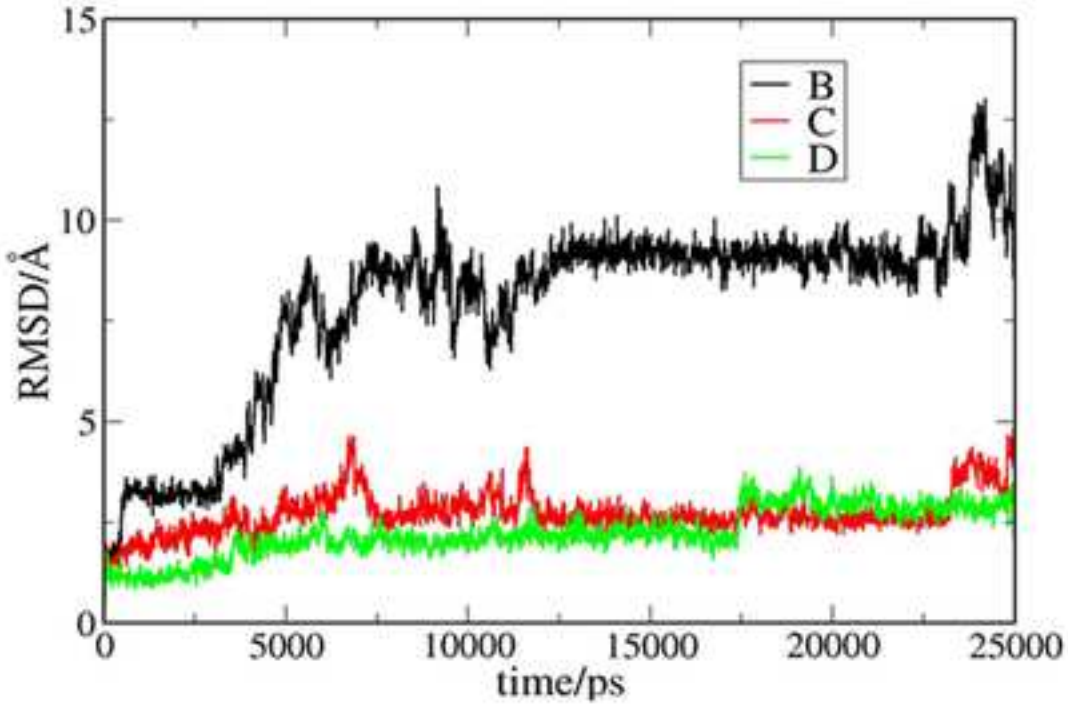

b)

Figure 6

Click here to download high resolution image

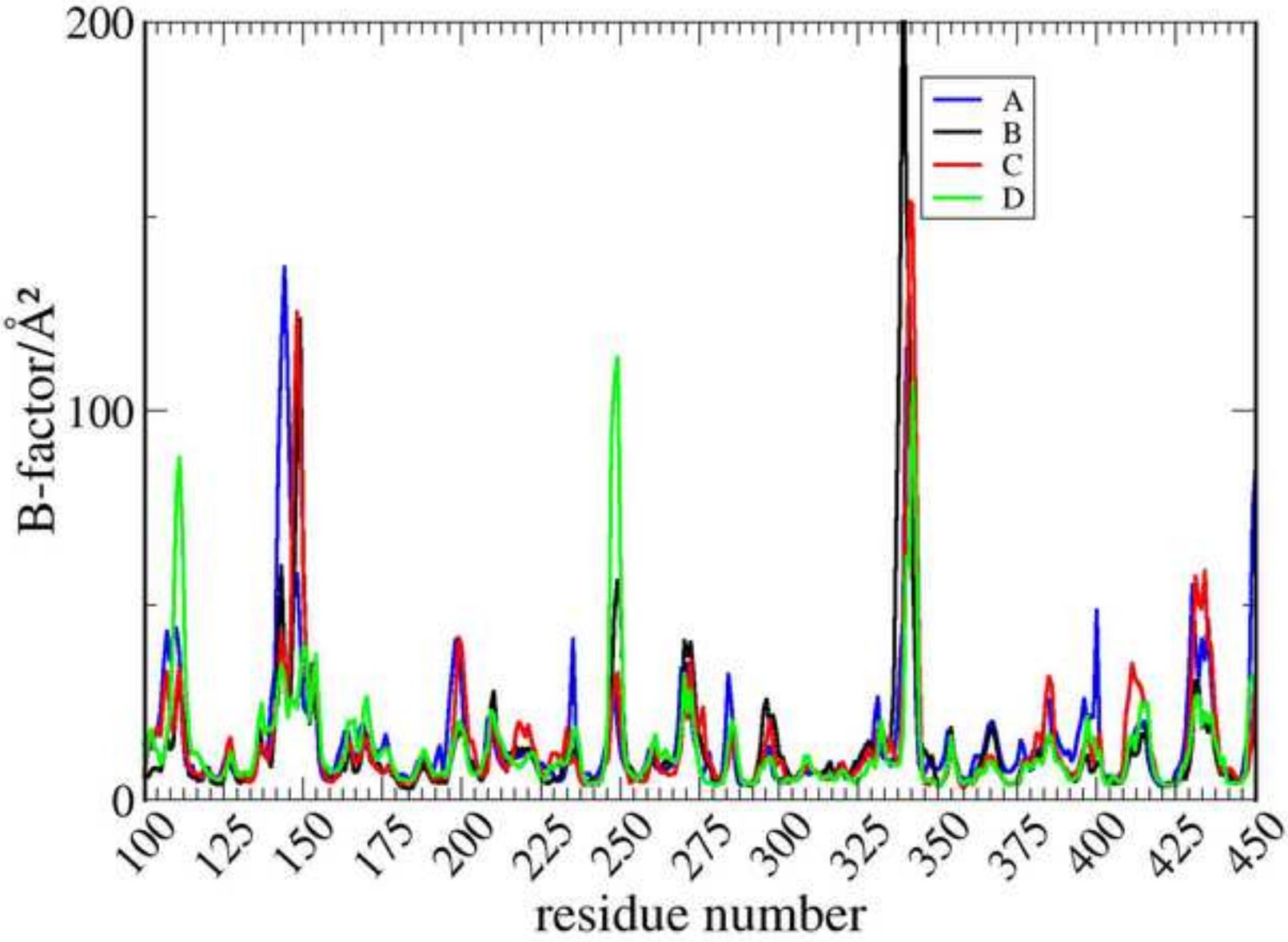

Figure 7

Click here to download high resolution image

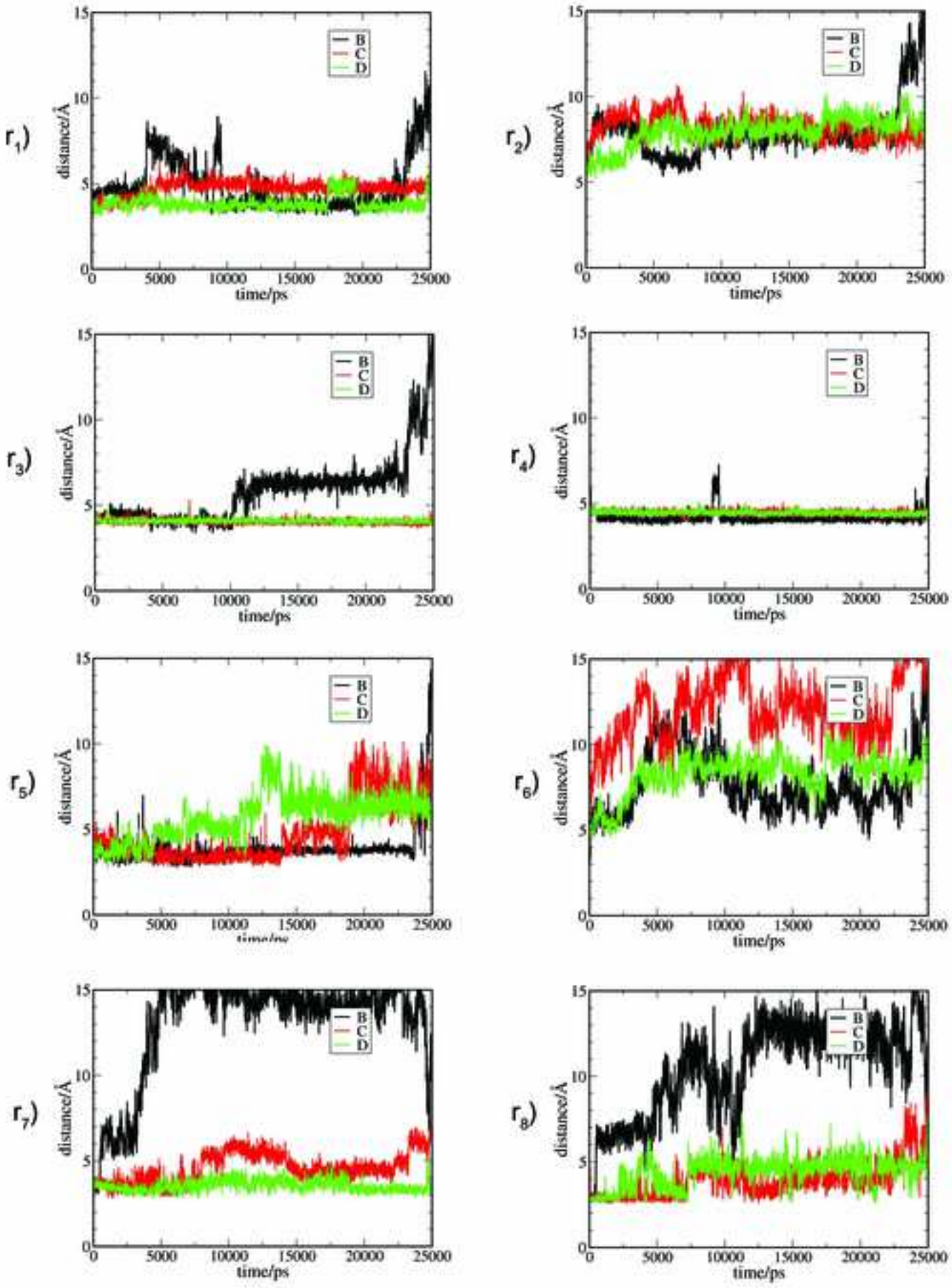

Figure 8

Click here to download high resolution image

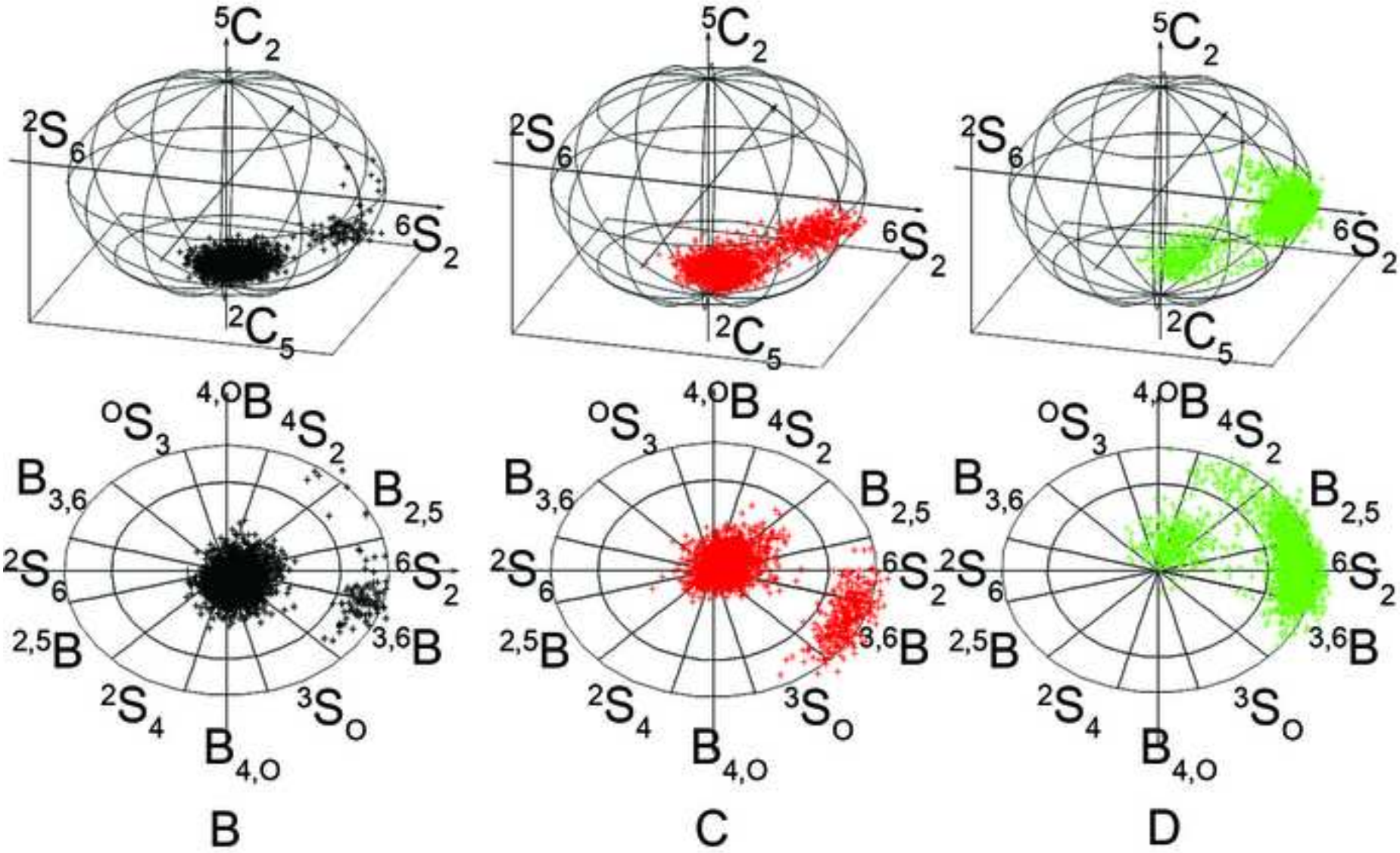

Figure 9
Click here to download high resolution image

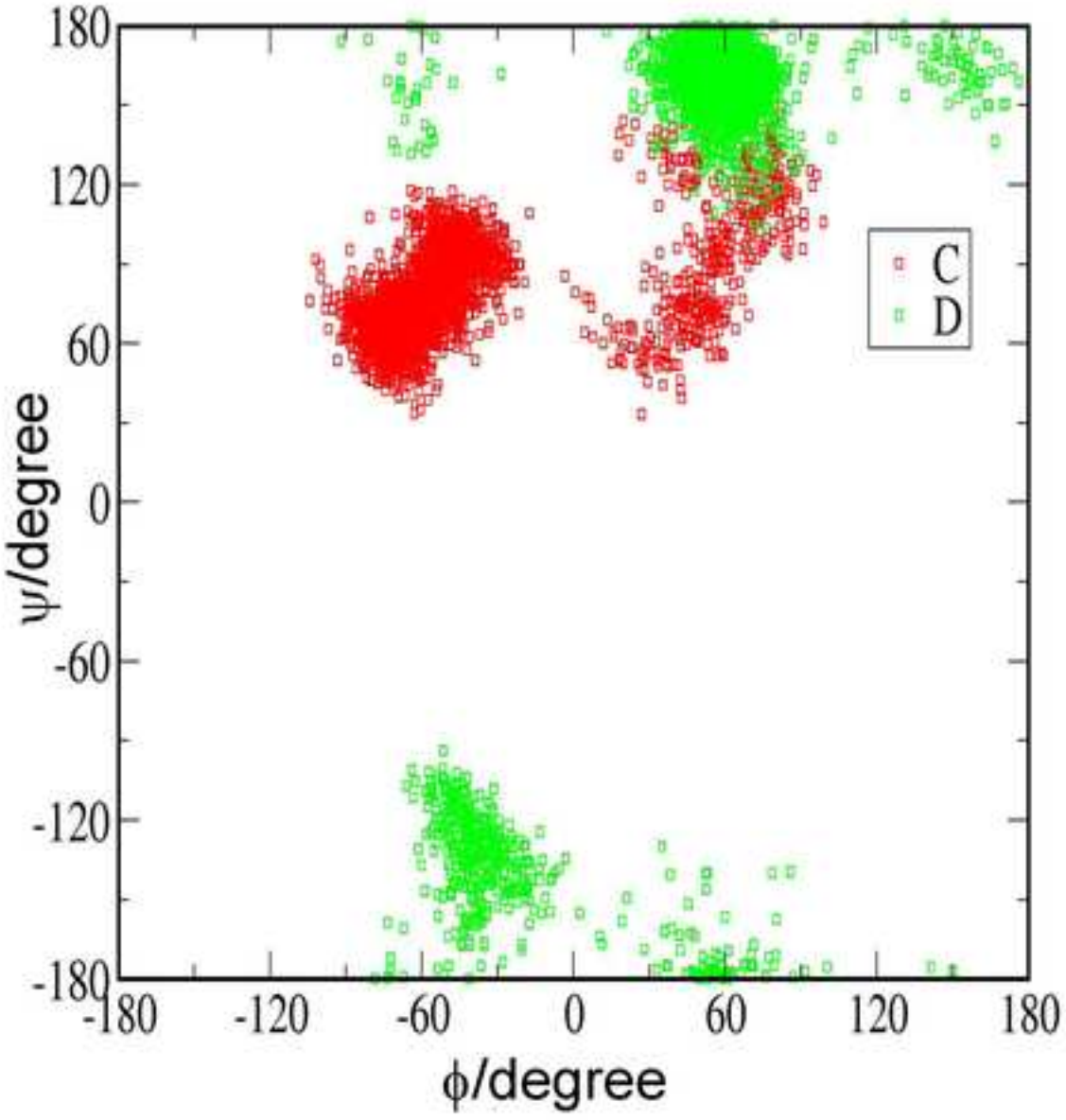

Figure 10
Click here to download high resolution image